Dynamics and spectroscopy of infrared-to-visible upconversion in erbium-doped cesium cadmium bromide ($CsCdBr_3:Er^{3+}$)

Nigel J. Cockroft
Los Alamos National Laboratory, Chemical and Laser Sciences Division, Mailstop J564, Los Alamos, New Mexico 87545

Glynn D. Jones
Department of Physics, University of Canterbury, Christchurch, New Zealand

Dinh C. Nguyen
Los Alamos National Laboratory, Chemical and Laser Sciences Division, Mailstop J564, Los Alamos, New Mexico 87545
(Received 22 April 1991; revised manuscript received 22 October 1991)

Trivalent erbium ions in $CsCdBr_3$ exist predominantly as dimers along one-dimensional lattice chains. Very efficient upconversion from near-infrared to various visible wavelengths was observed. $^2H_{9/2}\rightarrow{}^4I_{15/2}$ (414 nm) and $^4F_{7/2}\rightarrow{}^4I_{15/2}$ (493 nm) fluorescence dominated for $^4I_{15/2}\rightarrow{}^4I_{9/2}$ (801 nm) and $^4I_{15/2}\rightarrow{}^4I_{11/2}$ (984 nm) excitation, respectively. Simultaneous excitation at 801 and 984 nm preferentially populated $^4F_{5/2}$, giving $^4F_{5/2}\rightarrow{}^4I_{15/2}$ (455 nm), $^4F_{5/2}\rightarrow{}^4I_{13/2}$ (651 nm), and, by cross relaxation, $^4F_{9/2}\rightarrow{}^4I_{15/2}$ (671 nm). The efficiency of multiple-color upconversion is attributed to low phonon energies and close coupling between ions. Upconversion mechanisms are proposed, and energy-transfer rates determined from the temporal transients.

I. INTRODUCTION

In a recent paper two of us demonstrated efficient upconversion fluorescence for $^4I_{15/2}\rightarrow{}^4S_{3/2}$ excitation (547.47 nm) of erbium in $CsCdBr_3$.[1] This green cw excitation produced "white-light" Er^{3+} fluorescence that is comprised of many components in the region 338–870 nm. Additional fluorescence, outside of detector range, was inferred. High-resolution spectroscopy enabled assignment of levels to many manifolds and indicated that manifolds as high as $^4G_{9/2}$ at 36 150 cm^{-1} were populated. A complete energy transfer between two ions, both excited to the $E1$ level (18 247 cm^{-1} *in vacuo*) of the $^4S_{3/2}$ manifold, is required to achieve this in a dimer center. This mechanism was recently confirmed by McPherson and Meyerson[2] using pulsed green-laser excitation.

In this paper we report very efficient infrared-to-visible energy upconversion in Er^{3+}-doped $CsCdBr_3$. This is an infrared-to-visible-upconversion study that utilizes dimer-dominated materials. Three aspects of this upconversion are significant. First, the efficiency is much higher than for other hosts. Second, the strongest upconverted emission originates from Er^{3+} energy levels of higher energy than normally observed for pulsed near-infrared excitation. Finally, the emission wavelengths change if the pump manifold is changed. 801-nm ($^4I_{15/2}\rightarrow{}^4I_{9/2}$) excitation gives emission peaked at 414 nm ($^2H_{9/2}\rightarrow{}^4I_{15/2}$), whereas 984-nm ($^4I_{15/2}\rightarrow{}^4I_{11/2}$) excitation gives emission peaked at 493 nm ($^4F_{7/2}\rightarrow{}^4I_{15/2}$). Simultaneous 801- and 984-nm excitation gives strong emission at 455 nm ($^4F_{5/2}\rightarrow{}^4I_{15/2}$), 651 nm ($^4F_{5/2}\rightarrow{}^4I_{13/2}$), and 671 nm ($^4F_{9/2}\rightarrow{}^4I_{15/2}$). We account for each of these observations and conclude that this material is a good candidate for upconversion laser study.

II. BACKGROUND

$CsCdBr_3$, isomorphic with several AMX_3 crystals such as $CsNiCl_3$, has hexagonal symmetry and belongs to the $P63/mmc$ (D^4_{6h}) space group.[3] The structure has infinite linear chains of face-sharing $(Cd^{2+}Br_6^-)^{4-}$ octahedra along the crystallographic c axis. As the Cd^{2+}-ion separation along a chain is much less than the separation between chains, the structure can be considered, for many properties, to be one dimensional. The Cd^{2+} ions are located in sites of trigonal, D_{3d}, point-group symmetry.

In 1977 Henling and McPherson[4,5] demonstrated, by electron paramagnetic resonance (EPR) that trivalent rare-earth ions (R^{3+}) substituting Cd^{2+} ions in $CsCdBr_3$ preferentially form dimers. At least 90% of Gd^{3+} dopant ions form a center on the cadmium-ion chain of the type $-Cd^{2+}$-Gd^{3+}-V-Gd^{3+}-Cd^{2+}-, where V is a Cd^{2+} vacancy[4] and the Gd^{3+}-Gd^{3+} ion separation is 6.0 Å. This center is preferentially formed as it satisfies the charge-neutrality condition. Each Gd^{3+} ion in the pair has C_{3v} site symmetry. The analogous center occurs for each of the rare-earth ion dopants reported to date. Estimates of the dopant proportion forming this center include 93% for Nd^{3+} (Ref. 6) and 95% for Tb^{3+}.[7] A center comprising -Cd^{2+}-Nd^{3+}-Nd^{3+}-V-Cd^{2+}- has also been observed in small proportion.[8] In this center the two Nd^{3+} ions have nonequivalent crystal fields. Detailed Nd^{3+} spectroscopy has also revealed weak transitions due to two distinct "isolated" ion centers.[7,8]

The close proximity of dopant ions in the dimers makes $CsCdBr_3$ ideal for optical studies of energy

transfer. In addition to the Er^{3+} upconversion reports,[1,2] optical investigations include cross-relaxation quenching processes in Tb^{3+},[7,9] energy transfer from Ce^{3+} to Tm^{3+} in heterogeneous pairs,[10] several papers on the Nd^{3+} system,[6,8,11] high-resolution spectroscopy on Pr^{3+},[12] and observation of $4f$-to-$5d$ transitions of Ce^{3+}.[13] This type of charge-compensated dimer is also formed by trivalent transition-metal ions such as Cr^{3+} (Ref. 14) and Bi^{3+}.[15] If energy transfer within the dimer is not desired, a rare-earth ion can be codoped with a monovalent ion such as Li^+ or Na^+. In this case a charge-compensated dimer of the type $-Cd^{2+}$-R^{3+}-Na^+-Cd^{2+}- is preferentially formed.[16]

Motivation to understand and enhance upconversion processes has recently increased because of the availability of high-powered, near-infrared diode lasers. A solid-state blue-green laser pumped by diode lasers is desirable for applications such as underwater communication and optical-disk storage devices. One approach to this problem is to use a "two-color" sequential absorption process.[17] Upconversion by energy transfer between excited neighboring ions is an alternative approach which often uses a single near-ir pump source. Erbium is an ideal ion as it has visible emission and near-infrared absorption around 800 and 980 nm, both excellent diode-laser wavelengths. Low-temperature green ($^4S_{3/2} \rightarrow {}^4I_{15/2}$) upconversion laser action was first achieved in small, monolithic, Er^{3+}:$YLiF_4$ rods.[18] Less efficient laser action on other transitions in this material[19–21] and diode-pumping experiments[22] suggest the possibility of a multicolor solid-state laser.

Conventional laser materials such as $YLiF_4$ have nominally random distributions of rare-earth dopant. A high concentration (1–5 mol %) is required to obtain sufficient numbers of ions with suitable proximity to contribute to the upconversion process. Many ions do not contribute to upconversion and can result in loss by pump- and output-beam absorption. Such laser materials to date, have been small crystals (3–5 mm) that are monolithic.[18–22] For moderate pump powers the upconversion process in erbium preferentially populates the $^4S_{3/2}$ manifold for either 800- or 980-nm excitation.

The motivation for this study was to evaluate the efficiency of Er^{3+} infrared-to-visible fluorescence upconversion in a dimer-dominated material. Energy-transfer lasers using these materials should operate with lower dopant concentration than materials with random ion distribution. The relatively small phonon energies of $CsCdBr_3$ result in more efficient emission from more Er^{3+} manifolds than for typical oxide and fluoride hosts.

III. EXPERIMENT

Single crystals of erbium-doped $CsCdBr_3$ were prepared as previously described.[1] An erbium concentration of 1.0 mol % was used in the starting material, although some segregation usually occurs, causing a lower actual concentration.[1,6] Crystals of approximate dimension $3\times5\times5$ mm^3 were cleaved from the 6.5 mm$\times$2 cm boule. Samples were aligned so that pump-laser polarization was either parallel or perpendicular to the crystallographic c axis.

Fluorescence (unpolarized) was excited using two Quanta Ray Nd:YAG pumped-dye-laser systems. $^4I_{15/2} \rightarrow {}^4I_{11/2}$ excitation, around 980 nm, was provided by a DCR3 laser pumping LDS925 dye in a PDL3 dye laser. Typical pulse energies were 350 μJ with a duration of 8 nsec and a spectral bandwidth of about 0.01 Å at 980 nm. $^4I_{15/2} \rightarrow {}^4I_{9/2}$ excitation, around 800 nm, was provided by a DCR2 laser pumping LDS798 dye in a PDL1 dye laser. Typical pulse energies used were 1 mJ with duration of 10 nsec and spectral bandwidth of approximately 0.1–0.2 Å at 800 nm. Direct excitation of the $^4F_{3/2}$ and $^4F_{5/2}$ manifolds around 450 nm was achieved using Coumarin 440 dye in the PDL1 laser with a pulse energy of 150 μJ.

For the double-excitation experiments, the two near-infrared laser beams were coupled into the sample with a dichroic mirror. The delay between pulses was controlled electronically to an accuracy better than 1 nsec. The double-excitation spectra are unchanged for variation in relative time delay of up to 100 nsec and most measurements were made with the 801-nm pulse preceding the 984-nm pulse by 20 nsec.

Samples were cooled by a C.T.I. model 22C closed-cycle refrigerator. The temperature, as measured by a thermocouple at the sample head, was 10 K. The true sample temperature may be slightly higher, although the weak intensity of "hot bands" in the excitation spectra suggests that the temperature is quite close to that measured.

Fluorescence scans were recorded using a 1-m Spex 1704 monochromator and Stanford Research Systems SRS 250 gated boxcar integrator. The latter was

TABLE I. Energy levels (±0.5 cm^{-1}), *in vacuo*, of the principal Er^{3+} dimer center (the *A* center).

Level No.	$^4I_{15/2}$	$^4I_{13/2}$	$^4I_{11/2}$	$^4I_{9/2}$	$^4F_{9/2}$	$^4S_{3/2}$	$^2H_{11/2}$	$^4F_{7/2}$	$^4F_{5/2}$	$^4F_{3/2}$	$^2H_{9/2}$	$^4G_{11/2}$	$^4G_{9/2}$
1	0	6492.0	10157.5	12353.1	15130.0	18242.0	18965.0	20336.0	22008.3	22381.7	24389.8	26017.6	36140.5
2	31.0	6524.0	10158.5	12370.5	15148.3	18261.2	18970.5	20380.5	22010.9	22404.7	24396.1	26024.6	36144.5
3	62.9	6535.5	10175.0	12417.8	15213.8		19011.0	20401.5	22080.7		24416.4		
4	69.1	6544.0	10179.0	12435.2	15218.3		19078.5						
5	76.4	6651.5	10218.0	12469.6	15294.3		19111.5						
6	224.1	6653.5	10220.5				19125.0						
7	237.3												
8	241.7												

modified to give a maximum gate width of 160 μsec. Fluorescence transients were recorded on a Tektronix 11402 digitizing oscilloscope and analyzed using IGOR software on a Macintosh IIx computer.

Intensity measurements of spectra were made by monitoring the most intense transition in a spectrum using a boxcar gate width of 160 μsec and a delay chosen to sample the peak of the transient. The total spectrum intensity was obtained using temporal, spectral, and photomultiplier-tube (PMT) response-correction factors. The gate shape was integrated against the total transient, and the spectral fraction of the transition monitored, including allowance for the monochromator resolution, was determined. A Hamamatsu R955 photomultiplier tube was used for most experiments. The $^4I_{11/2}$ transients were recorded using a Hamamatsu 7102 tube cooled thermoelectrically to $-40\,^{\circ}$C.

Reference 1 reported energy levels in cm^{-1} as measured in air. Energies *in vacuo* are used here as they provide a more physical indication of energy mismatches important in energy-transfer processes. Table I contains energy levels determined in this study along with values converted (from primary data) from Ref. 1.

IV. RESULTS

A single Er^{3+} center we have labeled *A* dominates the spectroscopy of $CsCdBr_3:Er^{3+}$. In addition to detailed measurements of the upconversion spectra and temporal transients for this center, structure due to additional centers is surveyed.

A. Dominant center (the *A* center)

1. $^4I_{15/2} \rightarrow {}^4I_{9/2}$ excitation

Laser excitation of the $^4I_{9/2}$ levels resulted in efficient violet upconversion emission from $^2H_{9/2} \rightarrow {}^4I_{15/2}$. The excitation spectra of Fig. 1 were obtained by monitoring the strongest transition at 413.919 nm.

The two π-polarized transitions at 801.731 and 809.291 nm are considerably stronger than any of the σ-polarized transitions [Fig. 1(a)]. The 801.731-nm transition had a $\pi:\sigma$ polarization ratio of 11:1. However this small leakage is still sufficient to dominate the σ spectrum. Figures 1(b) and 1(c) are π and σ scans, respectively, expanded to enhance the weaker transitions. Each transition is labeled by its stronger polarization and the initial and terminating crystal-field level number. The larger numbers within a manifold indicate the higher-energy levels (Table I). Each transition was correlated to the dominant center by recording the $^2H_{9/2}$ transient. Only two $^4I_{9/2}$ levels were previously known. The remaining $^4I_{9/2}$ levels are identified from Fig. 1 and included in Table I.

The most intense fluoresence spectra obtained by excitation at 801.731 nm are given in Fig. 2. Figure 2(b) corresponds to the spectrum observed but not assigned to an Er^{3+} transition in Ref. 1, but instead attributed to a center tentatively assigned to traces of divalent samarium. No $^4I_{11/2}$ erbium levels have previously been reported. $^4I_{11/2}$ levels were identified from Fig. 2(c) and included in Table I.

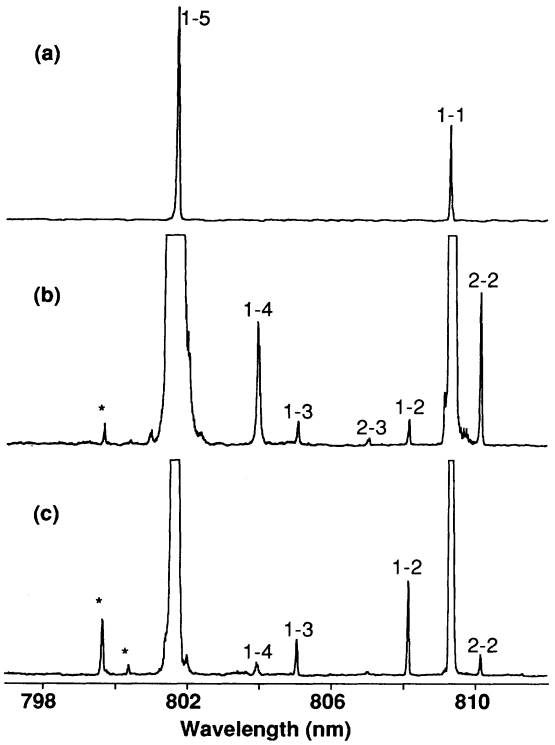

FIG. 1. $^4I_{15/2} \rightarrow {}^4I_{9/2}$ excitation spectra of the *A*-center monitoring upconverted $^2H_{9/2} \rightarrow {}^4I_{15/2}$ fluorescence at 413.919 nm: (a) π polarized, (b) π polarized, 1200 times expansion of (a), and (c) σ polarized, scale of (b). The asterisk indicates transitions of unknown origin.

Table II contains the relative intensities of the visible spectra observed for 1 mJ excitation. The most intense fluorescence originated from the $^2H_{9/2}$ manifold and branched to different ^4I manifolds. Very weak $^2H_{11/2} \rightarrow {}^4I_{15/2}$ was also observed, but was too weak to quantify (less than 0.001 on the scale of Table II) or to record an accurate transient. $^4G_{11/2} \rightarrow {}^4I_{15/2}$ emission (peaked at 387.585 nm) was also observed with an intensity of 0.06 on the scale of Table II.

The integrated $^2H_{9/2} \rightarrow {}^4I_{15/2}$ emission intensity was 27% that of nonupconverted $^4I_{9/2} \rightarrow {}^4I_{15/2}$ emission. The total visible upconversion fluorescence intensity for all of the spectral groups listed in Table II was 59% of the $^4I_{9/2} \rightarrow {}^4I_{15/2}$ emission.

Temporal transients for each of the upconverted manifolds observed for $^4I_{9/2}$ excitation are given in Fig. 3. Figure 3(a) includes a solid-line fit described in Sec. V C. The nonupconverted $^4I_{9/2}$ transient was single exponential with a lifetime of 11.1 msec.

2. $^4I_{15/2} \rightarrow {}^4I_{11/2}$ excitation

The strongest fluorescence spectrum for excitation of $^4I_{11/2}$ was $^4F_{7//2} \rightarrow {}^4I_{15/2}$, which peaks at 493.091 nm. The 10-K excitation spectra obtained by monitoring this transition are given in Fig. 4. The principal excitation transition is σ polarized at 984.244 nm.

TABLE II. Visible upconversion fluorescence intensities for the three excitation cases. The first columns contain normalized peak intensities for the transition monitored. The second columns give integrated intensities for each spectrum obtained by applying temporal, spectral and PMT response corrections to the peak intensities. Intensities in each column are normalized to a strongest value of 100.0.

	Intermanifold transition		$^4I_{9/2}$ excitation		$^4I_{11/2}$ excitation		Double excitation	
Spectrum	λ (nm)	Assignment	Peak int.	Total int.	Peak int.	Total int.	Peak int.	Total int.
$^2H_{9/2}$ to $^4I_{15/2}$	413.92	1-7	100.0	100.0	a	a	51.1	4.8
$^2H_{9/2}$ to $^4I_{13/2}$	563.80	1-5	5.3	49.6	a	a		2.4[b]
$^2H_{9/2}$ to $^4I_{11/2}$	703.31	1-3	14.3	50.3	a	a		2.4[b]
$^4F_{5/2}$ to $^4I_{15/2}$	455.78	2-5	0.16	1.8	a	a	40.0	9.4
$^4F_{5/2}$ to $^4I_{13/2}$	651.08	1-6		9.3[c]	a	a	100.0	48.0
$^4F_{7/2}$ to $^4I_{15/2}$	493.09	1-3	0.03	0.1	100.0	100.0	2.0	1.9
$^4F_{7/2}$ to $^4I_{13/2}$	722.15	1-1		0.004[d]	1.3	3.6		0.07[d]
$^4S_{3/2}$ to $^4I_{15/2}$	549.93	1-3	0.21	1.37	2.4	4.4	0.52	0.72
$^4F_{9/2}$ to $^4I_{15/2}$	671.29	1-7	0.50	3.52	11.1	22.8	54.7	100.0

[a]Not observed.
[b]Derived using branching ratios measured for the $^4I_{9/2}$ excitation case.
[c]Derived using branching ratios measured for the double-excitation case.
[d]Derived using branching ratios measured for the $^4I_{11/2}$ excitation case.

The excitation spectra show more structure than expected for a single dimer center. Upconverted fluorescence transients measured for excitation of the 984.244-nm transition are included in Fig. 5. The $^4F_{7/2}$ transient was used to identify transitions in Fig. 5 due to the A center. These transitions confirmed the $^4I_{11/2}$ levels determined from Fig. 2(c) and enabled identification of the missing level at 10220.5 cm^{-1} (Table I). The A-site $^4I_{11/2}$ emission has a single exponential lifetime determined to be 12.8 msec.

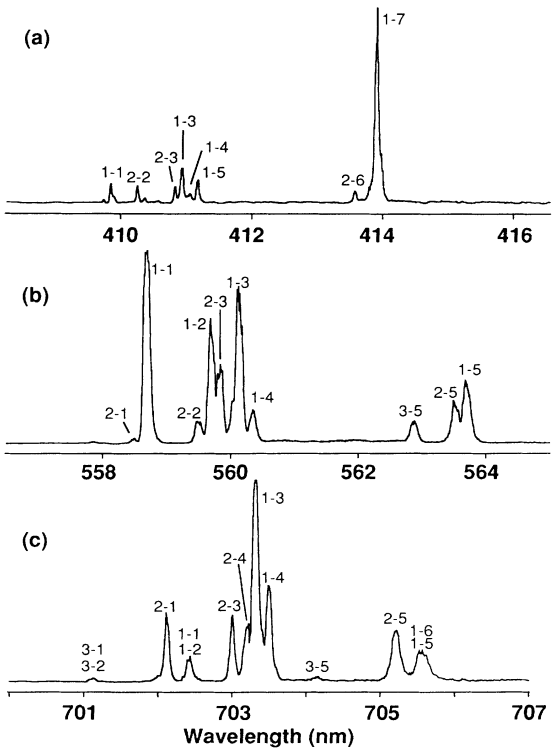

FIG. 2. Dominant upconverted fluorescence spectra observed for A-center $^4I_{15/2}\rightarrow{}^4I_{9/2}$ excitation (801.731 nm): (a) $^2H_{9/2}\rightarrow{}^4I_{15/2}$, (b) $^2H_{9/2}\rightarrow{}^4I_{13/2}$, and (c) $^2H_{9/2}\rightarrow{}^4I_{11/2}$.

Additional transitions, labeled J in Fig. 4, are due to a different center and will be discussed in detail elsewhere.

The relative intensities of the upconverted A-center fluorescence spectra for 984.244 nm excitation are included in Table II. Fluorescence from manifolds with energy higher than $^4F_{7/2}$ was not detected for 300 μJ excitation. A careful search gave an upper limit of 0.01% for the fluorescence intensity from any of these higher manifolds. The A-center $^4F_{7/2}\rightarrow{}^4I_{15/2}$ spectrum, the strongest observed for 984 nm excitation, is given in Fig. 6.

3. Double excitation

The upconversion fluorescence and dynamics were investigated for simultaneous (σ) 984 nm and (π) 801 nm excitation with incident energies of 350 and 650 μJ, respectively.

For this excitation case neither the $^2H_{9/2}\rightarrow{}^4I_{15/2}$ nor the $^4F_{7/2}\rightarrow{}^4I_{15/2}$ emissions were strongest. Instead, strong $^4F_{5/2}\rightarrow{}^4I_{15/2}$, $^4F_{5/2}\rightarrow{}^4I_{13/2}$, and $^4F_{9/2}\rightarrow{}^4I_{15/2}$ fluorescence, with strongest peaks at 455.776, 651.084, and 671.285 nm, respectively, was observed (Fig. 7).

Upconversion fluorescence transients of $^4F_{5/2}$, $^4S_{3/2}$, and $^4F_{9/2}$ for double excitation are included in Fig. 8. The $^2H_{9/2}$, $^4F_{7/2}$, and $^4I_{9/2}$ transients were not noticeably different from those for $^4I_{9/2}$ single excitation (Fig. 3). To confirm the double-excitation requirement of the $^4F_{5/2}$ and $^4F_{9/2}$ signals, we also recorded these transients, under the same conditions, for each single excitation. On the scale of Fig. 8(a), no $^4F_{5/2}$ emission is observable for either single-excitation case. The $^4F_{9/2}$ transient peak for each single-excitation case was approximately 2% that of Fig. 8(b).

Neither spectral intensities nor transients were changed when the 984- to 801-nm pump-laser-pulse separation was varied between +100 and −100 nsec.

The comparison of spectral intensity for double excitation depends on relative pump-radiation intensities, spatial pump-laser overlap, and the collection-optics configuration. Visual examination of the crystals indicated that the 801-nm laser, giving violet emission, had a greater penetration depth. The bright red, doubly excited, emission indicated that the overlap region was greatest within the first 2 mm. The fluorescence collection optics projected a line image, parallel to the direction of laser propagation, onto the monochromator slit axis. This captured the maximum excitation volume, but included the region where the 801-nm pump penetrated

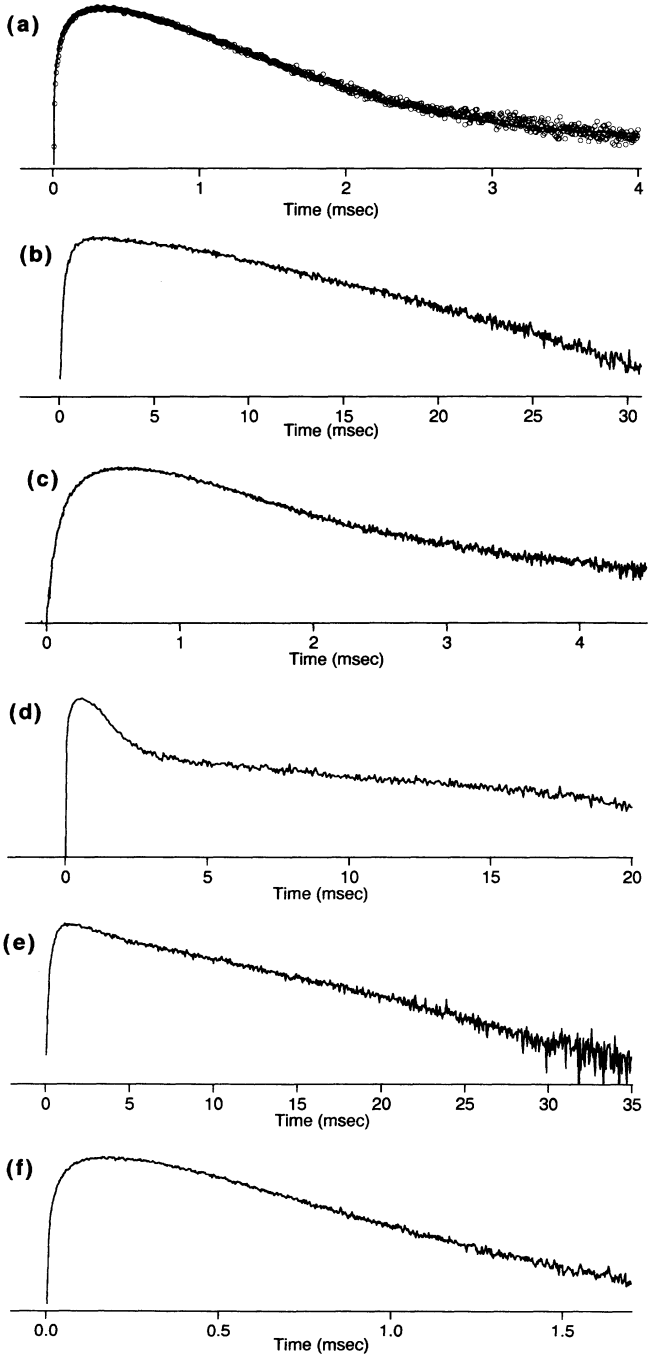

FIG. 3. Upconverted fluorescence transients for $^4I_{15/2} \rightarrow {}^4I_{9/2}$ A-center excitation (801.731 nm). The intensity scales are logarithmic. Wavelengths monitored are in parentheses: (a) $^2H_{9/2}$ (413.919 nm) [the solid-line fit to Eq. (4) is described in the text], (b) $^4F_{5/2}$ (651.084 nm), (c) $^4F_{7/2}$ (493.091 nm), (d) $^4S_{3/2}$ (549.931 nm), (e) $^4F_{9/2}$ (671.285 nm), and (f) $^4G_{11/2}$ (387.585 nm).

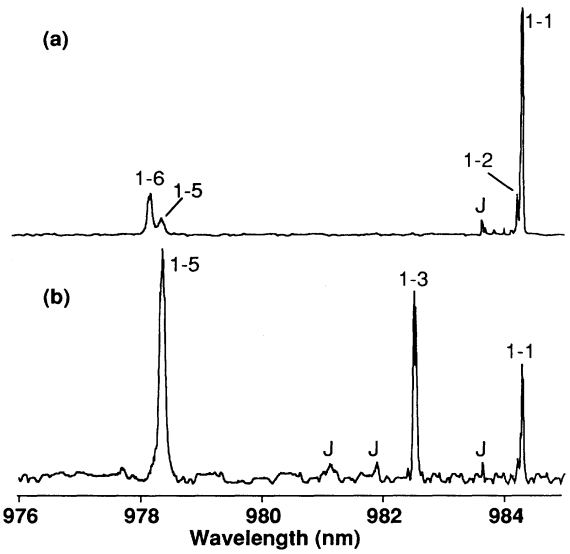

FIG. 4. $^4I_{15/2} \rightarrow {}^4I_{11/2}$ excitation spectra of the A-center monitoring upconverted $^4F_{7/2} \rightarrow {}^4I_{15/2}$ fluorescence at 493.091 nm (lines marked J are attributed to a different center): (a) σ polarized and (b) π polarized.

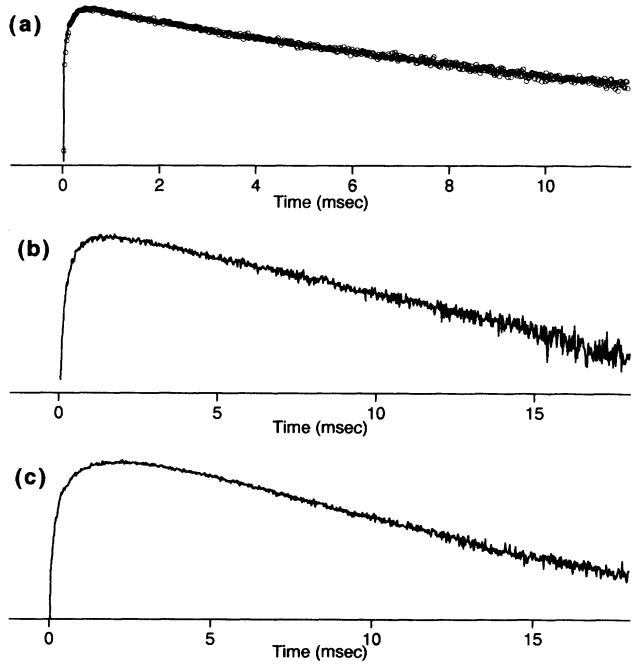

FIG. 5. Upconverted fluorescence transients for $^4I_{15/2} \rightarrow {}^4I_{11/2}$ A-center excitation (984.244 nm). The intensity scales are logarithmic. (a) $^4F_{7/2}$ (493.091 nm) [the solid line fit to Eq. (4) is described in the text], (b) $^4S_{3/2}$ (549.931 nm), and (c) $^4F_{9/2}$ (671.285 nm).

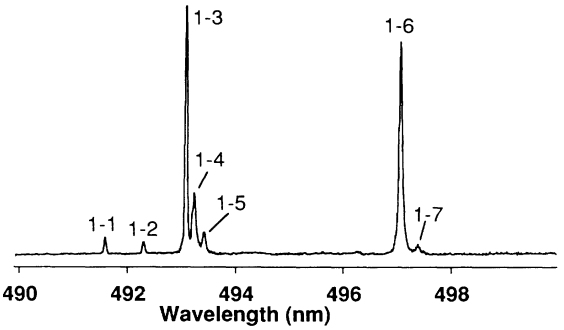

FIG. 6. Principal fluorescence spectrum $^4F_{7/2} \rightarrow {}^4I_{15/2}$ for $^4I_{15/2} \rightarrow {}^4I_{11/2}$ excitation (984.244 nm).

beyond the 984-nm pump.

Upconversion fluorescence for all three excitation cases was visually bright for excitation of the A center. Viewed through a blue pass filter, the crystal appeared violet (414 nm), blue/green (493 nm), or blue (455 nm) for 801-nm, 984-nm, or double excitation, respectively. Viewed with a red filter, the very bright red fluorescence (651 and 671 nm) for double excitation could be contrasted with the much weaker red fluorescence (671 nm) seen when either pump laser was blocked.

4. *Excited-state absorption*

When scanning the $^4I_{15/2} \rightarrow {}^4I_{9/2}$ excitation spectrum, a set of additional transitions was observed at longer wavelength (Fig. 9). Excitation at these wavelengths gave the same $^2H_{9/2} \rightarrow {}^4I_{15/2}$ fluorescence spectrum observed for $^4I_{15/2} \rightarrow {}^4I_{9/2}$ A-center excitation. The $^2H_{9/2}$ transient, however, exhibited a single exponential decay time of 266 μsec with no apparent rise time.

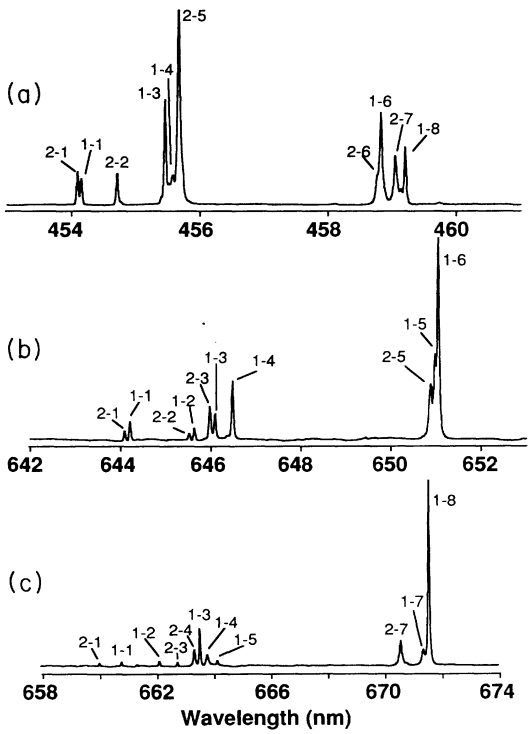

FIG. 7. Most intense upconverted A-center fluorescence spectra observed for double laser excitation (984.244 and 801.731 nm): (a) $^4F_{5/2} \rightarrow {}^4I_{15/2}$, (b) $^4F_{5/2} \rightarrow {}^4I_{13/2}$, and (c) $^4F_{9/2} \rightarrow {}^4I_{15/2}$.

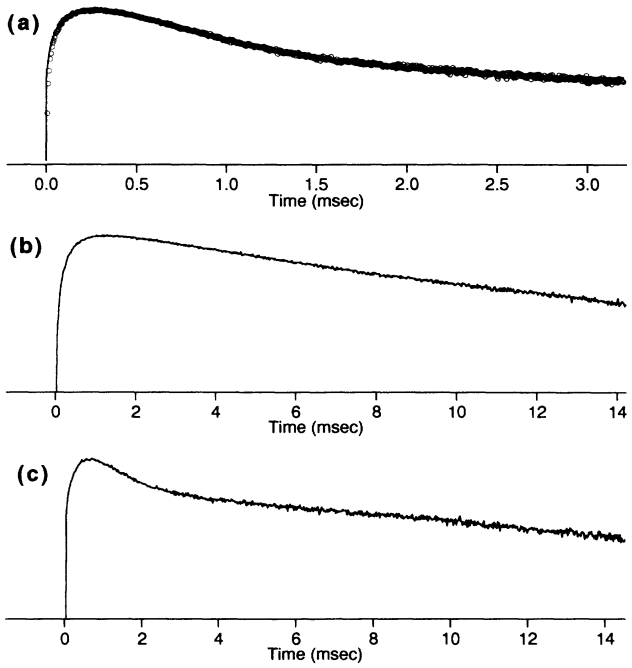

FIG. 8. Upconverted A-center fluorescence transients for double laser excitation (984.244 and 801.731 nm). The intensity scales are logarithmic. (a) $^4F_{5/2}$ (651.084 nm) [solid line fit to Eq. (4) is described in the text], (b) $^4F_{9/2}$ (671.285 nm), and (c) $^4S_{3/2}$ (549.931 nm).

The transition energies labeled in Fig. 9 identify these as $^4I_{9/2} \rightarrow {}^2H_{9/2}$ A-center excited-state absorption (ESA) transitions. This excitation mechanism was unexpected as the $^4I_{9/2}$ ion population is expected to be negligible. We attribute the initial excitation step $^4I_{15/2} \rightarrow {}^4I_{9/2}$ to an artifact of the dye-laser output. The peak of amplified spontaneous emission (ASE) from the LDS798 dye is close to the A-center 801-nm absorption peak. The ratio of ASE at 801 nm to laser-line energy increases considerably at the edge of the dye's tuning range. Although ASE at 801 nm has only 1.1% of the 820-nm laser energy, it is sufficient to account for the $^2H_{9/2}$ emission intensity. Integrated $^2H_{9/2} \rightarrow {}^4I_{15/2}$ emission by this excitation method was 0.11% that observed for $^4I_{15/2} \rightarrow {}^4I_{9/2}$ (801.7 nm) laser excitation.

5. $^4I_{15/2} \rightarrow {}^4F_{3/2}, {}^4F_{5/2}$ *excitation*

To assist the interpretation of cross-relaxation processes observed for double excitation, we examined emission for direct excitation of $^4F_{3/2}$ and $^4F_{5/2}$. An identical $^4F_{5/2}$ single exponential decay transient with a lifetime of 217 μsec was observed for both $^4I_{15/2} \rightarrow {}^4F_{5/2}$ and $^4I_{15/2} \rightarrow {}^4F_{3/2}$ pumping. There was no apparent rise time for either pump method, and no emission was observed

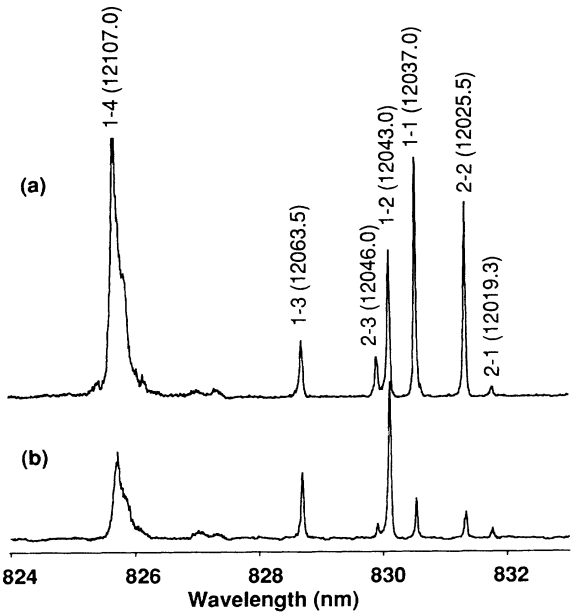

FIG. 9. Excited-state absorption ($^4I_{9/2} \rightarrow {}^2H_{9/2}$) excitation spectra monitoring upconverted A-center $^2H_{9/2} \rightarrow {}^4I_{15/2}$ fluorescence (413.919 nm): (a) π polarized and (b) σ polarized.

from $^4F_{3/2}$.

Efficient red emission of the $^4F_{5/2} \rightarrow {}^4I_{13/2}$ and $^4F_{9/2} \rightarrow {}^4I_{15/2}$ transitions was observed for either $^4F_{3/2}$ or $^4F_{5/2}$ excitation. The $^4F_{9/2} \rightarrow {}^4I_{15/2}$ emission was 6.6 times stronger than the $^4F_{5/2} \rightarrow {}^4I_{15/2}$ blue emission. The $^4F_{9/2}$ transient has a distinct exponential rise and decay component (Fig. 10). The solid-line fit is discussed in Sec. V C.

Excitation spectra confirmed the known $^4F_{3/2}$ levels,[1] but resulted in reassignment of the highest-energy $^4F_{5/2}$ level (Table I). The strongest $^4I_{15/2} \rightarrow {}^4F_{5/2}$ and $^4I_{15/2} \rightarrow {}^4F_{3/2}$ transitions are at 454.192 nm (π) and 446.209 nm (π), respectively, with the latter being 4 times the intensity of the former.

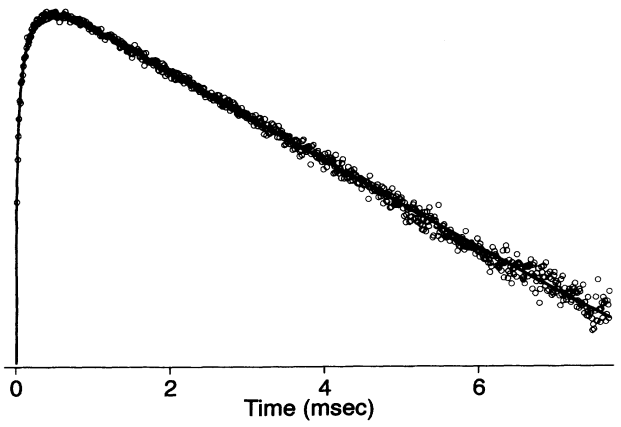

FIG. 10. A-center $^4F_{9/2}$ transient (monitoring 671.285 nm) for $^4I_{15/2} \rightarrow {}^4F_{5/2}$ excitation (454.246 nm). The intensity scale is logarithmic. The solid-line fit to Eq. (4) is described in the text.

6. *Unexplained A-center excitation mechanism*

Two weak transitions at 799.691 and 800.415 nm are marked by an asterisk in Figs. 1(b) and 1(c). Excitation at these wavelengths gave the same upconverted A-center $^2H_{9/2} \rightarrow {}^4I_{15/2}$ emission spectrum [Fig. 2(a)] as observed for resonant A-center $^4I_{15/2} \rightarrow {}^4I_{9/2}$ excitation. The $^2H_{9/2}$ transition, however, was substantially different. It comprised exponential rise and decay times of 29 and 261 μsec, respectively, compared with 226 and 521 μsec [Fig. 3(a)] for true $^4I_{9/2}$ excitation. As all of the A-center $^4I_{9/2}$ energy levels and transitions are accounted for, the origin of these additional transitions and the mechanism for upconversion is unknown. Integrated $^2H_{9/2} \rightarrow {}^4I_{15/2}$ fluorescence intensity for 799.691 nm excitation was 0.03% of that for resonant $^4I_{9/2}$ (801.731 nm) excitation.

B. Additional spectral structure assigned to minority centers

Some weak transitions in the excitation spectra are not from the A center. These transitions are due to eight minority centers, six of which exhibit upconversion, which are planned to be reported in more detail elsewhere.

V. DISCUSSION

Unusually efficient Er^{3+} emission is observed from many manifolds. This efficiency is attributed to small multiphonon relaxation rates resulting from the relatively low phonon energies of $CsCdBr_3$. Raman spectroscopy has revealed a highest phonon energy of 163.5 cm^{-1}.[23] Although infrared-absorption measurements may reveal additional vibrations of slightly higher energy, these values are expected to be relatively small compared with common oxides and fluorides. For example, the phonon cutoff energies of Y_2O_3 and CaF_2 are 560 cm^{-1} (Ref. 24) and 465 cm^{-1}.[25] The $^4F_{7/2}$ emission, for instance, reflects the consequence of these differences. The $^4F_{7/2} \rightarrow {}^2H_{11/2}$ energy gaps are 1211, 1103, and 1185 cm^{-1} for $CsCdBr_3$,[1] Y_2O_3,[26] and CaF_2 (Ref. 27) (A center), requiring at least eight, two, and three phonons, respectively, for multiphonon quenching. Since the decay probability is generally found to be exponential in phonon number,[28] the $^4F_{7/2}$ level is less strongly quenched and its emission much more efficient in $CdCdBr_3$. The 12-K direct-pumped lifetime is 210 μsec in $CsCdBr_2$,[1] less than 20 nsec in CaF_2,[29] and the emission is too weak to detect in Y_2O_3.[30]

The long lifetimes have significant consequences on the upconversion processes occurring in $CsCdBr_3$. In addition to allowing efficient visible emission after upconversion has occurred, the relatively long lifetimes of the metastable pump levels allow *different* upconversion pathways to those normally observed.

A. *A*-center configuration

If comparable oscillator strengths are assumed, it can be inferred from the excitation and absorption spectra

that approximately 95% of the Er^{3+} ions exist in the *A*-center configuration. The efficient upconversion reported here and in Ref. 1 requires a close proximity of Er^{3+} ions for this center. Two charge-compensated Er^{3+} dimers are possible (Sec. II). The optical-absorption spectra are consistent with a predominant single set of Er^{3+}-ion crystal-field levels.[1] We therefore attribute the dominant center to the $-Cd^{2+}-Er^{3+}-V-Er^{3+}-Cd^{2+}-$ configuration in which both Er^{3+} ions experience the same crystal field. This assignment is consistent with observations for other rare-earth dopants.[4,6,7] The alternative $-Cd^{2+}-Er^{3+}-Er^{3+}-V-Cd^{2+}-$ comprises two erbium ions in different crystal fields and has distinct transitions from each ion type.

B. Upconversion spectroscopy and mechanisms

The observation of violet upconversion is unusual for pulsed excitation and is best understood by contrasting with a more conventional Er upconversion host. In Er:$YLiF_4$ pulsed excitation to either $^4I_{9/2}$ or $^4I_{11/2}$ results in efficient $^4S_{3/2}\rightarrow{}^4I_{15/2}$ emission. The mechanism attributed to $^4I_{11/2}$ pumped upconversion is a total transfer between two ions in this state to excite one ion into $^4F_{7/2}$. In $YLiF_4$, however, this ion decays *nonradiatively* to emit preferentially from the $^4S_{3/2}$ level (green emission).[18] The latter fluorescence is also dominant for $^4I_{9/2}$ excitation as efficient multiphonon decay feeds the pump excitation from $^4I_{9/2}\rightarrow{}^4I_{11/2}$ followed by the same upconversion mechanism. High-powered cw excitation may result in higher-order processes[19–21] that give shorter wavelengths, but are less significant for pulsed excitation.

In $CsCdBr_3$ none, one, or both ions in the dimer may be excited by the pump pulse with upconversion fluorescence occurring only for the latter case. The upconversion mechanisms proposed for $^4I_{9/2}$, $^4I_{11/2}$, and double excitation are shown in Figs. 11(a)–11(c).

The very long lifetime of the $^4I_{9/2}$ manifold (11.1 msec at 10 K) and the close ion proximity in the dimer configuration enable an efficient transfer of the type

$$(^4I_{9/2},{}^4I_{9/2})\rightarrow(^4I_{15/2},{}^2H_{9/2}),$$

for $^4I_{9/2}$ (801 nm) excitation. Once excited to the $^2H_{9/2}$ manifold, the ions decay radiatively to the ^4I manifolds as the multiphonon quenching rate is small. The energy mismatch for this upconversion process would require the emission of, at most, two phonons. Only the lowest three of five $^2H_{9/2}$ levels, spanning 26.6 cm^{-1}, have been identified (Table I). The mismatch for transfer to the highest known level is 290 cm^{-1}. Transfer to higher, as-yet unknown, $^2H_{9/2}$ levels is expected to result in a much smaller energy mismatch. The total $^2H_{9/2}$ splitting in Er:$YLiF_4$ is 227 cm^{-1}.[31] Although the smaller crystal field of $CsCdBr_3$ will produce a smaller splitting, by comparison with other manifolds we expect a total $^2H_{9/2}$ splitting of at least 160 cm^{-1}. This would result in an energy mismatch small enough to require the emission of only a single phonon.

A careful search detected no $^4I_{11/2}\rightarrow{}^4I_{15/2}$ emission for the case of $^4I_{9/2}$ excitation. This confirms the lack of multiphonon feeding to this level at 10 K. If this level had been populated, we would expect to see more intense components of $^4F_{5/2}$ and $^4F_{7/2}$ emission through the processes depicted in Figs. 11(b) and 11(c).

Very weak emission is observed from $^4G_{11/2}\rightarrow{}^4I_{15/2}$ (Sec. IV A 1). As this level is more than twice the energy of the $^4I_{9/2}$ pump level, we attribute this observation to energy transfer *between centers*. This may occur if dimers on a chain are in close proximity or if dimers on neighboring chains are adjacent to each other. This seems more likely than the *A*-center dimer undergoing full upconversion energy transfer then absorbing a third photon within the 10-nsec duration of the pump-laser pulse. A concentration dependence study would help identify the mechanism involved.

The upconversion mechanism proposed for $^4I_{11/2}$ excitation [Fig. 11(b)] requires a total-energy transfer between two excited ions in a dimer:

$$(^4I_{11/2},{}^4I_{11/2})\rightarrow(^4I_{15/2},{}^4F_{7/2}),$$

as proposed for other hosts. In $CsCdBr_3$ the $^4F_{7/2}$ level decays radiatively to give the dominant 493-nm emission. Using the $^4I_{11/2}$ and $^4F_{7/2}$ levels of Table I, the energy mismatch is close to zero. For example, the transfer between two ions in the lowest $^4I_{11/2}$ level requires absorption of a 21-cm^{-1} phonon to reach the lowest $^4F_{7/2}$ level. Alternatively, transfer for a dimer with ions in the second and third lowest $^4I_{11/2}$ levels has only a 2.5-cm^{-1} energy mismatch with the lowest $^4F_{7/2}$ level. Several other Stark-level combinations require only small phonon-energy dissipations for this upconversion process.

The results of the double-excitation experiments are also unique to this material. We attribute the preferential population of the $^4F_{5/2}$ level to dimers which are heterogeneously excited, as shown in Fig. 11(c). One ion of the dimer is excited to $^4I_{9/2}$ by the 801-nm laser, while the other is excited to $^4I_{11/2}$ with the 984-nm laser. Either ion can transfer to the other:

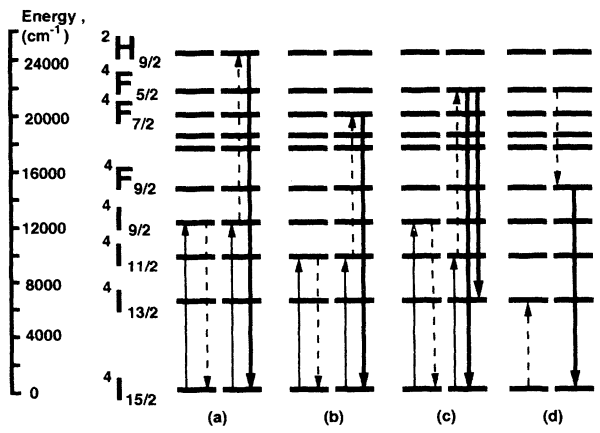

FIG. 11. Upconversion mechanisms for dimers in $CsCdBr_3$:Er^{3+}: (a) $^2H_{9/2}$ population by $^4I_{9/2}$ excitation, (b) $^4F_{7/2}$ population by $^4I_{11/2}$ excitation, (c) $^4F_{5/2}$ population by $^4I_{9/2}$ plus $^4I_{11/2}$ excitation, and (d) $^4F_{9/2}$ population by $^4F_{5/2}$ cross relaxation.

$$({}^4I_{9/2},{}^4I_{11/2})\rightarrow({}^4F_{3/2},{}^4I_{15/2})$$

or

$$({}^4I_{11/2},{}^4I_{9/2})\rightarrow({}^4F_{3/2},{}^4I_{15/2})\ .$$

For ions in the lowest-energy states of their respective manifolds, most likely at 10 K, the mismatch requires the emission of a single 106-cm^{-1} phonon. We propose that multiphonon decay to the ${}^4F_{5/2}$ level (across a 300-cm^{-1} gap) quenches any emission from ${}^4F_{3/2}$ and results in ${}^4F_{5/2}$ emission. Direct excitation of ${}^4F_{3/2}$ confirmed that no ${}^4F_{3/2}$ emission was observable (Sec. IV A 5). The fact that ${}^4F_{5/2}$ and ${}^4F_{9/2}$ transients were identical for either ${}^4F_{3/2}$ or ${}^4F_{5/2}$ direct excitation, along with the lack of any appreciable ${}^4F_{5/2}$ rise time, confirms very rapid multiphonon decay from ${}^4F_{3/2}$.

The observation that the red ${}^4F_{9/2}\rightarrow{}^4I_{15/2}$ emission for double near-infrared excitation is more than 20 times as intense as the sum of the ${}^4F_{9/2}$ emission intensities for the two single near-infrared excitation cases is also attributed to cross relaxation between ions in the dimer. Multiphonon feeding is ruled out by the lack of enhancement of other levels between ${}^4F_{5/2}$ and ${}^4F_{9/2}$ (Table II). The cross-relaxation mechanism of Fig. 11(d) is proposed to account for direct feeding of the ${}^4F_{9/2}$ manifold. In order to achieve the ${}^4F_{5/2}$ population by the mechanism of Fig. 11(c), the second ion in the dimer must be in the ${}^4I_{15/2}$ state. Transfer then occurs by

$$({}^4F_{5/2},{}^4I_{15/2})\rightarrow({}^4F_{9/2},{}^4I_{13/2})\ ,$$

with small mismatch. For ions in the lowest levels of the ${}^4F_{5/2}$ and ${}^4I_{15/2}$ manifolds transferring to the highest levels of the ${}^4F_{9/2}$ and ${}^4I_{13/2}$ manifolds (Table I), phonon emission of just 60.5 cm^{-1} is required.

The efficient emission from ${}^4F_{9/2}$ for direct ${}^4F_{5/2}$ or ${}^4F_{3/2}$ excitation (Secs. IV A 5 and V C) verified the cross-relaxation mechanism of Fig. 11(d). This mechanism has also been observed for an Er^{3+} dimer in CaF_2.[32]

The unexpected observation of ${}^4I_{9/2}\rightarrow{}^2H_{9/2}$ excited-state absorption is relevant to the discussion here for two reasons. First, the two-step absorption process simulates a direct ${}^2H_{9/2}$ excitation process since both photons originate within the same fast pulse. This gives a value for the ${}^2H_{9/2}$ lifetime used in the dynamics analysis. Second, the observation indicates that two-step excitation using two lasers may be a very efficient upconversion process. This would be very useful where pulsed excitation to other levels of manifolds higher than the 24 390-cm^{-1} lowest level of the ${}^2H_{9/2}$ manifold is desired. Dimers doubly excited to ${}^4I_{9/2}$ by one laser could have one ion excited with an 825-nm pulse to levels of the ${}^2H_{9/2}$ manifold. Energy transfer of the type

$$({}^4I_{9/2},{}^2H_{9/2})\rightarrow({}^4I_{15/2},{}^4G_{9/2})$$

would result in ${}^4G_{9/2}\rightarrow{}^4I_{15/2}$, ${}^4I_{13/2}$, and ${}^4I_{11/2}$ emission at 278, 338, and 386 nm, respectively.

C. Dynamics of the *A* center

$CsCdBr_3$ is an ideal host for the study of energy transfer. In most hosts energy-transfer observations comprise a convolution of different rates resulting from variable radial separations of randomly distributed dopants. These separations must be averaged in some way, thereby reducing the certainty of the information derived.

As the Er^{3+} ions in the one distinct Er-*V*-Er dimer center present have the same interion separation, there is a single rate for each energy-transfer process. Although not directly measured here, the Er^{3+}-ion separation is expected to be close to the 6.0-Å value measured for Gd^{3+}.[4]

Energy-transfer rates can be derived from the upconverted fluorescence transients of Figs. 3 and 5. Figure 12 gives a generalized representation of the upconversion processes shown in Fig. 11. In each case the two ions of the dimer are excited by the pump laser to state 2 and then interact to give one ion in state 3, while deexciting the other.

The temporal dependence of state-3 populations N_3 depends on the transfer rate W_t between the two ions in state 2.

Buisson and Vial[33] considered upconversion in dimers using a population N_d representing dimers in which both ions are excited. N_d has an initial population produced by the laser pulse, which decreases both through the upconversion energy-transfer process, with rate W_t, and through the intrinsic decay rate of the pumped state, with rate W_2. Accounting for the latter requires a factor of 2 since decay of either ion deexcites the dimer:

$$\dot{N}_d=-2W_2N_d-W_tN_d\ . \tag{1}$$

The upper-state population is given by

$$\dot{N}_3=W_tN_d-W_3N_3\ , \tag{2}$$

where W_3 is the intrinsic decay rate of level 3 and W_t is the upconversion energy-transfer rate. Solution of Eqs. (1) and (2) gives

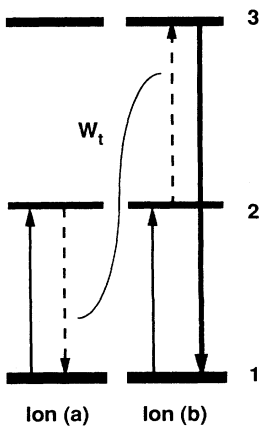

FIG. 12. Generalized upconversion scheme for the two ions in a dimer.

$$N_3 = \frac{N_d^0 W_t}{[W_3 - (2W_2 + W_t)]}(e^{-(2W_2+W_t)t} - e^{-W_3 t}) , \quad (3)$$

where N_d^0 is the initial population of excited dimers.

Equation (3) describes a transient with an exponential rise and decay. The decay rate is the lesser of W_3 or $(2W_2 + W_t)$, and the greater of the two rates describes the rise. Table II shows that each excitation case studied preferentially populated a single upper state. Upconverted transients have been fitted to an expression, for the intensity,

$$I = A + B(e^{-Ct} - e^{-Dt}) , \quad (4)$$

for each excitation case.

1. $^4I_{15/2} \rightarrow {}^4I_{9/2}$ excitation

The simple mechanism for populating $^2H_{9/2}$ [Fig. 11(a)] is ideal for analysis with Eq. (3). N_1, N_2, and N_3 are the populations of $^4I_{15/2}$, $^4I_{9/2}$, and $^2H_{9/2}$, respectively.

An excellent fit over the entire transient yields a rise rate [C in Eq. (4)] of 4425 sec^{-1} and a decay rate [D in Eq. (4)] of 1921 sec^{-1}. This fit is the solid line on the data in Fig. 3(a). No direct pump measurement of W_3, the intrinsic $^2H_{9/2}$ decay rate, has been made, but the choice of assignment of rate C or D to W_3 is aided by the excited-state absorption measurements (Sec. IV A). ESA, which simulates direct excitation of $^2H_{9/2}$, gave a single exponential decay time of 266 μsec ($W = 3760$ sec^{-1}). On this basis we correlate the observed rise time of Fig. 3(a) to W_3. Consequently, $D = 2W_2 + W_t = 1921$ sec^{-1} and W_t could be determined if the intrinsic $^4I_{9/2}$ lifetime were known. The following argument is used to justify a probable value of 90.1 sec^{-1} for W_2.

Whereas upconverted fluorescence occurs only from dimers in which both ions have been excited, the $^4I_{9/2}$ emission may originate from ions in dimers in which the neighboring ion is not excited. The directly excited exponential decay time observed for $^4I_{9/2}$ emission was 11.1 msec ($W = 90.1$ sec^{-1}). We believe this decay rate represents the singly excited dimers, rather than the upconversion-quenched doubly excited dimers, for the following reasons.

(a) The pump energies used did not saturate the absorption transition. The probability for single excitation is therefore greater than for double excitation.

(b) The bandwidth of the 801-nm transition in excitation spectra obtained by monitoring $^4I_{9/2}$ emission was 1.4 (close to $\sqrt{2}$) times wider than that observed when monitoring upconverted emission. This is expected from the quadratic dependence on the absorption cross section for the double excitation of a dimer. Emission observed for excitation on the transition wings definitely originates from the singly excited dimers. The $^4I_{9/2}$ transient observed was identical whether pumped at the wings or the transition peak.

(c) The absolute intensity and transient of $^4I_{9/2}$ emission did not change noticeably when the $^4I_{11/2}$ excitation laser was turned on in the double-excitation experiments. This indicates the existence of a large reservoir of singly excited dimers.

Using the above assumption, then, W_2 is taken to be 90.1 sec^{-1} and the transfer rate W_t is estimated to be 1741 sec^{-1}.

2. $^4I_{15/2} \rightarrow {}^4I_{11/2}$ excitation

The best fit to Eq. (4) is superposed on the upconverted $^4F_{7/2}$ transient of Fig. 5(a) and yields rise and decay rates C and D of 5605 and 284.3 sec^{-1}, respectively.

The directly excited lifetime for the $^4F_{7/2}$ manifold is 210 μsec.[1] This is correlated to the upconverted rise time of 178 μsec ($W = 5605$ sec^{-1}). Therefore,

$$D = 2W_2 + W_t = 284.3 \text{ sec}^{-1} .$$

Using the same arguments as described for the $^4I_{9/2}$ excitation case, the observed $^4I_{11/2}$ decay rate (Sec. IV A 2) of 78.1 sec^{-1} is used as the probable value for W_2. The upconversion energy-transfer rate W_t is therefore estimated to be 128.3 sec^{-1}. This is almost an order of magnitude less than the value of 1741 sec^{-1} estimated for the $^4I_{9/2}$ excitation upconversion process of Fig. 11(a).

3. Double excitation

The double-excitation case is more complex for four reasons.

(a) The decay rates of two intermediate states $^4I_{9/2}$ and $^4I_{11/2}$ are involved.

(b) Two processes are possible:

$$(^4I_{9/2}, {}^4I_{11/2}) \rightarrow (^4F_{3/2}, {}^4I_{15/2})$$

and

$$(^4I_{11/2}, {}^4I_{9/2}) \rightarrow (^4F_{3/2}, {}^4I_{15/2}) ,$$

which may have different transfer rates.

(c) The $^4F_{3/2}$ manifold, which is initially populated by the upconversion mechanism, does not emit, but relaxes to the $^4F_{5/2}$ manifold whose emission must be analyzed.

(d) There is an efficient cross-relaxation mechanism which feeds population from $^4F_{5/2}$ to the $^4F_{9/2}$ manifold [Fig. 11(d)].

Equation (3) can be modified to account for this situation. The direct pumping of $^4F_{3/2}$ showed no apparent rise time on the $^4F_{5/2}$ transient, suggesting that transfer to this level is rapid enough to use the $^4F_{5/2}$ transient as level 3 in the model. We now assume that the $^4I_{9/2} \rightarrow {}^4I_{11/2}$ and $^4I_{11/2} \rightarrow {}^4I_{9/2}$ upconversion transfer rates are equal and label this rate W_{TA}. We replace the $2W_2$ term [Eqs. (1) and (3)] with $W_{2i} + W_{2ii}$, the $^4I_{9/2}$ and $^4I_{11/2}$ intrinsic decay rates, respectively. The transfer rate depopulating $^4F_{5/2}$ by the mechanism of Fig. 11(d) is labeled W_{TB}.

Equations (2) and (3) become

$$\dot{N}_3 = W_{TA} N_d - (W_3 + W_{TB}) N_3 , \quad (5)$$

$$N_3=\frac{N_d^0 W_{\mathrm{TA}}}{(W_3+W_{\mathrm{TB}})-(W_{2i}+W_{2ii}+W_{\mathrm{TA}})} \times(e^{-(W_{2i}+W_{2ii}+W_{\mathrm{TA}})t}-e^{-(W_3+W_{\mathrm{TB}})t}) , \quad (6)$$

where N_d^0 is the number of dimers in the excited state $({}^4I_{9/2},{}^4I_{11/2})$.

Equation (6) has the same form as Eq. (4). Figure 8(a) includes the best ${}^4F_{5/2}$ fit obtained with rise and decay rates of 6231 and 2110 sec^{-1}, respectively. Direct excitation of ${}^4F_{5/2}$ gave a decay rate of 4608 sec^{-1}. We correlate this to the 6231-sec^{-1} rise time with the difference between these values being accounted for in the next section on ${}^4F_{5/2}$ direct pumping. Therefore, $D=2110\ \mathrm{sec}^{-1}=W_{2i}+W_{2ii}+W_{\mathrm{TA}}$. Substituting the ${}^4I_{9/2}$ and ${}^4I_{11/2}$ rates for direct pumping, the upconversion transfer rate W_{TA} for the mechanism of Fig. 11(c) is estimated to be 1942 sec^{-1}, slightly greater than the value of 1741 sec^{-1} for ${}^4I_{9/2}$ single-excitation case.

4. ${}^4I_{15/2}\rightarrow{}^4F_{3/2},{}^4F_{5/2}$ excitation: Cross relaxation

Direct blue excitation was examined to help understand the observation of the strong red ${}^4F_{9/2}\rightarrow{}^4I_{15/2}$ emission for double-excitation upconversion. Tallant, Miller, and Wright[32] proposed the cross-relaxation mechanism of Fig. 11(d) to account for a similar observation for ${}^4F_{5/2}$ excitation of an erbium dimer in CaF_2. The same mechanism is invoked here for the A center in $CsCdBr_3{:}Er^{3+}$.

If labels 1, 2, 3, and 4 represent the ${}^4I_{15/2}$, ${}^4I_{13/2}$, ${}^4F_{9/2}$, and ${}^4F_{5/2}$ manifolds, then, for direct pulsed excitation of ${}^4F_{5/2}$,

$$\dot{N}_4=-W_4N_4-W_{\mathrm{TB}}N_4 , \quad (7)$$

$$\dot{N}_3=W_{\mathrm{TB}}N_4-W_3N_3 . \quad (8)$$

Therefore,

$$N_4=\frac{N_4^0}{(W_4+W_{\mathrm{TB}})}e^{-(W_4+W_{\mathrm{TB}})t} \quad (9)$$

and

$$N_3=\frac{N_d^0 W_{\mathrm{TA}}}{(W_4+W_{\mathrm{TB}})-W_3}(e^{-W_3t}-e^{-(W_4+W_{\mathrm{TB}})t}) , \quad (10)$$

where W_3 and W_4 are intrinsic decay rates, W_{TB} is the cross-relaxation energy-transfer rate for the mechanism of Fig. 11(d), and N_{40} is the population of ions initially excited to the ${}^4F_{5/2}$ state by the laser pulse.

Equation (9) predicts a single exponential decay for the ${}^4F_{5/2}$ level which was observed to be 4608 sec^{-1} for 150 μJ direct excitation. The discrepancy with the inferred value of 6231 sec^{-1} from the double near-ir excitation experiment is explained by the fact that the observed transients arise from an ensemble of excited dimers. In the double-excitation case, all dimers with an ion in the ${}^4F_{5/2}$ state must initially have the neighbor in the ${}^4I_{15/2}$ state according to the upconversion mechanism of Fig. 11(c). Each excited dimer is therefore available to participate in the cross-relaxation mechanism of Fig. 11(d). For direct excitation, however, some dimers are doubly excited by the laser to the $({}^4F_{5/2},{}^4F_{5/2})$ state and are unable to undergo the ${}^4F_{9/2}$ cross relaxation. The contribution to the decay rate of the W_{TB} term is therefore reduced, and the ${}^4F_{5/2}$ lifetime is increased. Data from the current experiments do not enable the separate determination of the W_4 and W_{TB} rates.

The reduction of cross-relaxation efficiency caused by the presence of $({}^4F_{5/2},{}^4F_{5/2})$ dimers is also reflected in the red $({}^4F_{9/2}\rightarrow{}^4I_{15/2})$ to blue $({}^4F_{5/2}\rightarrow{}^4I_{15/2})$ emission intensity ratio. This ratio was ≈ 11 for double excitation (Table II) and only 6.6 for direct ${}^4F_{5/2}$ excitation.

Equation (10) predicts a rise and decay of the form of Eq. (4). Figure 10 is the ${}^4F_{9/2}$ transient observed for direct ${}^4F_{5/2}$ excitation. The superposed best fit to Eq. (4) gave decay and rise times of 554 and 4866 sec^{-1}. The latter is in good agreement with the W_4+W_{TB} rate observed for directly excited ${}^4F_{5/2}$ emission. The decay rate is therefore attributed to W_3 and predicts a ${}^4F_{9/2}$ lifetime of 1.8 msec.

VI. CONCLUSION

The predominance of Er^{3+} dimers in $CsCdBr_3$ results in very efficient near-infrared–to–visible upconversion. Fluorescence from many manifolds occurs as a result of the host lattice having relatively low phonon energies. An unusually long ${}^4I_{9/2}$ lifetime, together with the small ($\sim$6 Å) separation of Er^{3+} ions aids energy transfer between two excited ions to populate the ${}^2H_{9/2}$ manifold. The resultant 414-nm fluorescence for pulsed excitation is much more efficient than for comparable Er^{3+} concentrations in randomly distributing hosts such as $YLiF_4$ and $YAlO_3$

The constant ion separation for the A-center dimer gives a single energy-transfer rate which is easily deconvoluted from the temporal transients. Upconversion energy-transfer rates for dimers in the $({}^4I_{9/2},{}^4I_{9/2})$, $({}^4I_{11/2},{}^4I_{11/2})$, and $({}^4I_{9/2},{}^4I_{11/2})$ states were examined to be 1742, 128, and 1942 sec^{-1}, respectively. Excellent fits of the data to a single-rate model suggest that $CsCdBr_3$ and isomorphs could be used as a tool for investigating energy-transfer rates between other ion combinations under study as upconversion laser systems.

Preliminary survey results have indicated that the

small proportion of Er^{3+} ions not present in the *A*-center dimer are distributed between a large number of centers. Detailed dynamics studies planned for these centers may also reveal further interesting energy-transfer behavior.

The efficient short-wavelength upconversion and the unusual tunability between violet, blue-green, and red emission by appropriate choice of excitation pump wavelength indicates that $CsCdBr_3:Er^{3+}$ may make a versatile diode-pumped upconversion laser system.

ACKNOWLEDGMENTS

We thank George Faulkner for technical assistance and discussions. This work was supported by the Institutionally Supported Research and Development (I.S.R.D.) program of the Los Alamos National Laboratory and performed under the auspices of the Department of Energy.

[1]N. J. Cockroft, G. D. Jones, and R. W. G. Syme, J. Lumin. **43**, 275 (1989).
[2]G. L. McPherson and S. L. Meyerson, Chem. Phys. Lett. **167**, 471 (1990).
[3]G. L. McPherson, A. M. McPherson, and J. L. Atwood, J. Phys. Chem. Solids **41**, 495 (1980).
[4]L. M. Henling and G. L. McPherson, Phys. Rev. B **16**, 4756 (1977).
[5]G. L. McPherson and L. M. Henling, Phys. Rev. B **16**, 1889 (1977).
[6]R. B. Barthem, R. Buisson, F.. Madeore, J. C. Vial, and J. P. Chaminade, J. Phys. (Paris) **48**, 379 (1987).
[7]P. A. M. Berdowski, M. J. J. Lammers, and G. Blasse, J. Chem. Phys. **83**, 476 (1985).
[8]C. Barthou and R. B. Barthem, J. Lumin. **46**, 9 (1990).
[9]M. J. J. Lammers and G. Blasse, Chem. Phys. Lett. **126**, 405 (1986).
[10]A. M. McPherson and G. L. McPherson, Solid State Commun. **37**, 501 (1981).
[11]R. B. Barthem, R. Buisson, J. C. Vial, and J. P. Chaminade, J. Phys. (Paris) Colloq. **46**, C7-113 (1985); R. B. Barthem, R. Buisson, and R. L. Cone, J. Chem. Phys. **91**, 627 (1989).
[12]J. P. Chaminade, R. M. Macfarlane, F. Ramaz, and J. C. Vial, J. Lumin. **48-49**, 531 (1991).
[13]G. Blasse, A. Wolfert, and G. L. McPherson, J. Solid State Chem. **57**, 396 (1985).
[14]G. L. McPherson, Wai-ming Heung, and J. J. Barraza, J. Am. Chem. Soc. **100**, 469 (1978).
[15]A. Wolfert and G. L. Blasse, J. Solid State Chem. **55**, 344 (1984).
[16]G. L. McPherson and A. H. Francis, Phys. Rev. Lett. **41**, 1681 (1978).
[17]D. C. Nguyen, G. E. Faulkner, and M. Dulick, Appl. Opt. **28**, 3553 (1989).
[18]W. Lenth, A. J. Silversmith, and R. M. Macfarlane, in *Advances in Laser Science–III,* Proceedings of the Third International Laser Science Conference, Atlantic City, NJ, November 1–4, 1987, edited by Andrew C. Tam, James L. Gole, and William C. Stwalley, AIP Conf. Proc. No. 172 (AIP, New York, 1988), p. 8.
[19]R. A. McFarlane, Appl. Phys. Lett. **54**, 2301 (1989).
[20]R. A. McFarlane, M. Robinson, and S. A. Pollack, Proc. Soc. Photo-Opt. Instrum. Eng. **1223**, 294 (1990).
[21]T. Hebert, R. Wannemacher, W. Lenth, and R. M. Macfarlane, Appl. Phys. Lett. **57**, 1727 (1990).
[22]F. Tong, W. P. Risk, R. M. Macfarlane, and W. Lenth, Electron. Lett. **25**, 1391 (1989).
[23]C. W. Tomblin, G. D. Jones, and R. W. G. Syme, J. Phys. C **17**, 4345 (1984); O. Pilla, E. Cazzanelli, B. Blanzat, C. Andraud, and F. Pelle, Phys. Status Solidi B **144**, 845 (1987).
[24]N. T. McDevitt and A. D. Davidson, J. Opt. Soc. Am. **56**, 636 (1966).
[25]M. M. Elcombe and A. W. Pryor, J. Phys. C **3**, 492 (1970).
[26]J. B. Gruber, W. F. Krupke, and J. M. Poindexter, J. Chem. Phys. **41**, 3363 (1964).
[27]C. A. Freeth, G. D. Jones, and R. W. G. Syme, J. Phys. C **15**, 5667 (1982).
[28]M. J. Weber, Phys. Rev. **171**, 283 (1968).
[29]M. P. Miller and J. C. Wright, J. Chem. Phys. **71**, 324 (1979).
[30]B. M. Tissue, N. J. Cockroft, L. Lu, D. C. Nguyen, and W. M. Yen, J. Lumin. *48-49*, 477 (1991).
[31]M. R. Brown, K. G. Roots, and W. A. Shand, J. Phys. C **2**, 593 (1969).
[32]D. R. Tallant, M. P. Miller, and J. C. Wright, J. Chem. Phys. **65**, 510 (1976).
[33]R. Buisson and J. C. Vial, J. Phys. (Paris) Lett. **42**, L115 (1981).